



# OPEN Stocks and fluxes of carbon and nitrogen in northeastern Brazil coastal seascapes

Antoniwal A. Jatobá-Junior<sup>1</sup>✉, Pere Masque<sup>2,3</sup>, Carlos Eduardo de Rezende<sup>4</sup> & Vanessa Hatje<sup>1,3</sup>

Quantifying carbon and nitrogen dynamics is essential for understanding the role of coastal ecosystems in climate change mitigation and habitat connectivity. We assessed organic carbon (OC) and total nitrogen (TN) stocks, accumulation rates, and isotopic composition ( $\delta^{13}\text{C}$  and  $\delta^{15}\text{N}$ ) in sediment across diverse seascapes in northeastern Brazil, including high- and low-salinity mangroves, a tidal flat, a freshwater marsh, and an inundated forest. OC stocks in the upper meter of sediment were highest in the freshwater marsh ( $283 \pm 64 \text{ Mg OC ha}^{-1}$ ) and tidal flat ( $266 \pm 27 \text{ Mg OC ha}^{-1}$ ), and were comparable to mangroves ( $239 \pm 11$  to  $263 \pm 44 \text{ Mg OC ha}^{-1}$ ), while the inundated forest stored less ( $138 \text{ Mg OC ha}^{-1}$ ). Accumulation rates were highest in the marsh ( $202 \pm 19 \text{ g OC m}^{-2} \text{ yr}^{-1}$ ) and in the high-salinity mangroves ( $187 \pm 20 \text{ g OC m}^{-2} \text{ yr}^{-1}$ ), with lower values in tidal flats ( $108 \pm 3 \text{ g OC m}^{-2} \text{ yr}^{-1}$ ), inundated forests ( $119 \text{ g OC m}^{-2} \text{ yr}^{-1}$ ), and low-salinity mangroves ( $105 \pm 11 \text{ g OC m}^{-2} \text{ yr}^{-1}$ ). TN stocks ranged from  $7.7 \text{ Mg N ha}^{-1}$  (inundated forest) to  $18.9 \text{ Mg N ha}^{-1}$  (marsh), with intermediate values in mangroves ( $8.3$ – $11.6 \text{ Mg N ha}^{-1}$ ) and the tidal flat ( $13.5 \text{ Mg N ha}^{-1}$ ). TN accumulation rates mirrored those of OC, being highest in the marsh ( $12.4 \pm 3.9 \text{ g N m}^{-2} \text{ yr}^{-1}$ ) and lowest in low-salinity mangroves ( $3.6 \pm 1.4 \text{ g N m}^{-2} \text{ yr}^{-1}$ ). Isotopic signatures reflected the dominance of  $\text{C}_3$  vegetation, but also highlighted the limited discriminatory power of stable isotopes alone, emphasizing the need for complementary tracers (e.g., fatty acids, pyrolysis, or eDNA) to resolve OM sources across seascapes. Overall, substantial OC and N storage in both vegetated and unvegetated habitats highlights the need to broaden Blue Carbon policies to include tidal flats and inland wetlands within Blue Carbon frameworks and management strategies.

**Keywords** Organic carbon stocks, Fluxes of organic matter, Isotopic ratios, Habitat connectivity, Seascape interactions

Coastal vegetated ecosystems (CVE), including mangroves, salt marshes, and seagrasses, are found along coastlines worldwide, except in Antarctica. These ecosystems are pivotal in shaping coastal morphology, safeguarding shorelines against erosion, providing food and shelter for numerous species, and acting as vital interfaces between marine and terrestrial environments. They are also referred to as Blue Carbon (BC) ecosystems, since they play a significant role in climate regulation by sequestering carbon, offering nature-based solutions for mitigating greenhouse gas emissions<sup>1–3</sup>. These ecosystems are recognized in IPCC guidelines (Wetland Supplement 2014), which support the inclusion of CVE management in national greenhouse gas inventories. Beyond accounting, the active protection, restoration, and expansion of these ecosystems are key to enhancing their  $\text{CO}_2$  sequestration capacity and ensuring the long-term stability of their carbon stocks. Such actions not only contribute to achieving the global climate mitigation targets of the Paris Agreement but also sustain biodiversity and a wide range of ecosystem services that underpin coastal resilience and human well-being.

Like tropical evergreen forests, CVE are highly productive and capture atmospheric  $\text{CO}_2$ , storing it as organic carbon (OC). This OC can remain stored in both aboveground and belowground biomass, such as leaves, stems, and roots, as well as in soil, where it accumulates over time<sup>1,4</sup>. The combination of fine-grained and waterlogged

<sup>1</sup>Centro Interdisciplinar de Energia e Ambiente, Universidade Federal da Bahia, Salvador, Brazil. <sup>2</sup>School of Sciences & Centre for Marine Ecosystems Research, Edith Cowan University, 270 Joondalup Drive, Joondalup, WA 6027, Australia. <sup>3</sup>IAEA Marine Environment Laboratories, Department of Nuclear Sciences and Applications, International Atomic Agency, Monaco, Principality of Monaco. <sup>4</sup>Laboratório de Ciências Ambientais, Centro de Biotecnologias e Biotecnologia, Universidade Estadual do Norte Fluminense Darcy Ribeiro, Campos dos Goytacazes, Brazil. ✉email: junicaugusto@gmail.com

sediments along with anoxic conditions favors slow decomposition rates, preserving OC for timescales ranging from decades to millennia<sup>1,5,6</sup>. However, it is important to mention that microbial decomposition still occurs naturally, releasing some OC back to the atmosphere mainly as CO<sub>2</sub> and CH<sub>4</sub><sup>7,8</sup>. Additionally, anthropogenic impacts can also enhance OC mineralization, thereby increasing greenhouse gas emissions to the atmosphere<sup>9–11</sup>.

CVE are directly influenced by hydrodynamic forces such as tidal pumping, which facilitate the transport of organic matter (OM) across the seascape<sup>11–13</sup>. In mangroves, up to 50% of the litterfall that accumulates on the forest floor can be washed away by tides and exported as particulate organic matter and litter to nearby ecosystems<sup>12,14</sup>. Additionally, recent studies suggest that a significant fraction of the carbon sink in mangrove forests and saltmarshes may be attributed to the outwelling of porewater-derived dissolved inorganic carbon (DIC) to adjacent ecosystems<sup>12,13,15–18</sup>. In contrast, benthic organisms such as crabs can remove and consume over 25–70% of annual mangrove litterfall, significantly retaining organic matter within the forest and reducing tidal export<sup>19,20</sup>. Therefore, dynamics in these ecosystems are not only driven by local primary production but also by the exchange of organic matter and nutrients with adjacent habitats, highlighting the need to evaluate ecosystems as interconnected components of the seascape mosaic rather than isolated units. The concept of seascape connectivity refers to the physical and biological linkages that allow the transfer of organic matter, nutrients, and energy across habitats, generating cross-habitat subsidies that enhance ecosystem functioning and biogeochemical cycling<sup>21</sup>.

Studies on seagrass-mangroves seascapes indicate that seagrass soils often store OC predominantly derived from mangroves<sup>21–24</sup>. For example, Chen<sup>23</sup>, estimated that up to ~80% of buried OC in seagrass meadows in North Sulawesi (Indonesia) originated from adjacent mangroves. Conversely, tidal flows and mangrove root structures facilitate the trapping of suspended sediment and OM from adjacent environments<sup>25</sup>. The relative contributions of OM sources to mangrove soils, including inputs from seagrasses, salt marshes, macroalgae, and terrestrial environments, vary widely depending on geomorphology, hydrology, and seasonal cycles<sup>21,26–29</sup>.

While CVE are important carbon-rich systems, their role in nitrogen cycling is equally significant and more complex. Wetlands can act both as nitrogen sources and sinks, depending on hydrology, vegetation, and microbial community structure<sup>30</sup>. Microbial pathways such as ammonification, nitrification, denitrification, and dissimilatory nitrate reduction operate simultaneously in soils, governed by redox gradients and organic matter availability<sup>31,32</sup>. The alternation between aerobic and anaerobic microsites, common in mangrove and marsh sediments, promotes these transformations and enables wetlands to mitigate nitrogen pollution<sup>33</sup>. Moreover, wetland connectivity plays a fundamental role in regulating nutrient transport and transformation across the landscape. Hydrological and biological connections among mangroves, marshes, and tidal flats increase the residence time of nitrogen in the system, enhancing opportunities for retention via sedimentation and microbial processing<sup>21</sup>. Given that anthropogenic pressures such as eutrophication can shift wetlands from nitrogen sinks to sources, a deeper understanding of nitrogen dynamics is crucial for managing these systems as multifunctional blue carbon seascapes.

The strong connectivity of CVE drives a complex interplay of organic matter from both local (autochthonous) and external (allochthonous) sources, with this complexity increasing as more contributing habitats are involved. Recent study suggests that much of the organic carbon stored in CVE may originate from allochthonous sources rather than the habitat-forming plants themselves<sup>34</sup>. Since, in general, most of the OC in CVE is stored belowground, accurately identifying, and quantifying the contributions from different sources is essential for understanding carbon dynamics and storage potential. This is not only relevant for ecological studies but also for climate mitigation efforts, as Blue Carbon ecosystems are increasingly being integrated into carbon markets and national greenhouse gas inventories. In this context, assessing autochthonous OC serves as a proxy for the CO<sub>2</sub> sequestration potential of a given habitat and helps avoid the risk of double counting carbon sequestration in carbon credit assessments<sup>27</sup>. Despite advancements in using tracers such as isotopes, accurately tracing OM exchanges across habitats remains challenging and most of the studies are constrained to the upper centimeters of sediment and focus primarily on mangrove-seagrass systems.

In this study we address gaps in understanding the dynamics of OC and TN accumulation across a continuous seascape. We quantified OC and TN stocks and accumulation rates in soils from various habitats, including two mangroves, a tidal flat, a freshwater marsh, and an inundated forest. Through δ<sup>13</sup>C and δ<sup>15</sup>N analysis in soil and plant tissues (leaves, stems, and roots), we aimed to identify the sources of OC and TN in soils and explore potential biogeochemical linkages among these ecosystems. We also aimed to investigate changes in OC inputs and accumulation rates over time using <sup>210</sup>Pb dating of sediment cores. This approach could provide a temporal perspective on the contribution of the various habitats to OC and TN storage. We hypothesize that connectivity across the coastal seascape, driven by hydrodynamic transport of particulate and dissolved organic matter, habitat export of detritus and nutrients and biogeochemical transformations, plays a key role in the transfer of OC and TN between habitats. These mechanisms are expected to influence the spatial patterns of carbon and nitrogen stocks, and to shape the isotopic composition of C and N in soils across various habitats, providing insights into the seascape-scale interactions that may regulate organic matter dynamics.

## Methods

### Study area and sampling design

This study was conducted along the seascapes of the Itapicuru River (Fig. 1) in the municipality of Conde (11°47'S, 37°33'W), Bahia, northeastern Brazil. The Itapicuru River basin covers an area of 36,000 km<sup>2</sup>, encompassing fifty-six cities with a population of around 1.6 million<sup>35</sup>. Despite deforestation caused by road construction and agriculture over the past century, the estuary remains well-preserved within the Environmental Protection Area of the North Coast of Bahia (APA/LN)<sup>36</sup>. In Conde, small villages like Siribinha and Poças, each with ~500 inhabitants, primarily rely on fishing<sup>37</sup>. The region has a tropical-humid climate, with an average temperature of 25°C and annual precipitation of 1,400 mm<sup>38</sup>. The tidal regime is semidiurnal, ranging from 2.0 to 2.5 m.

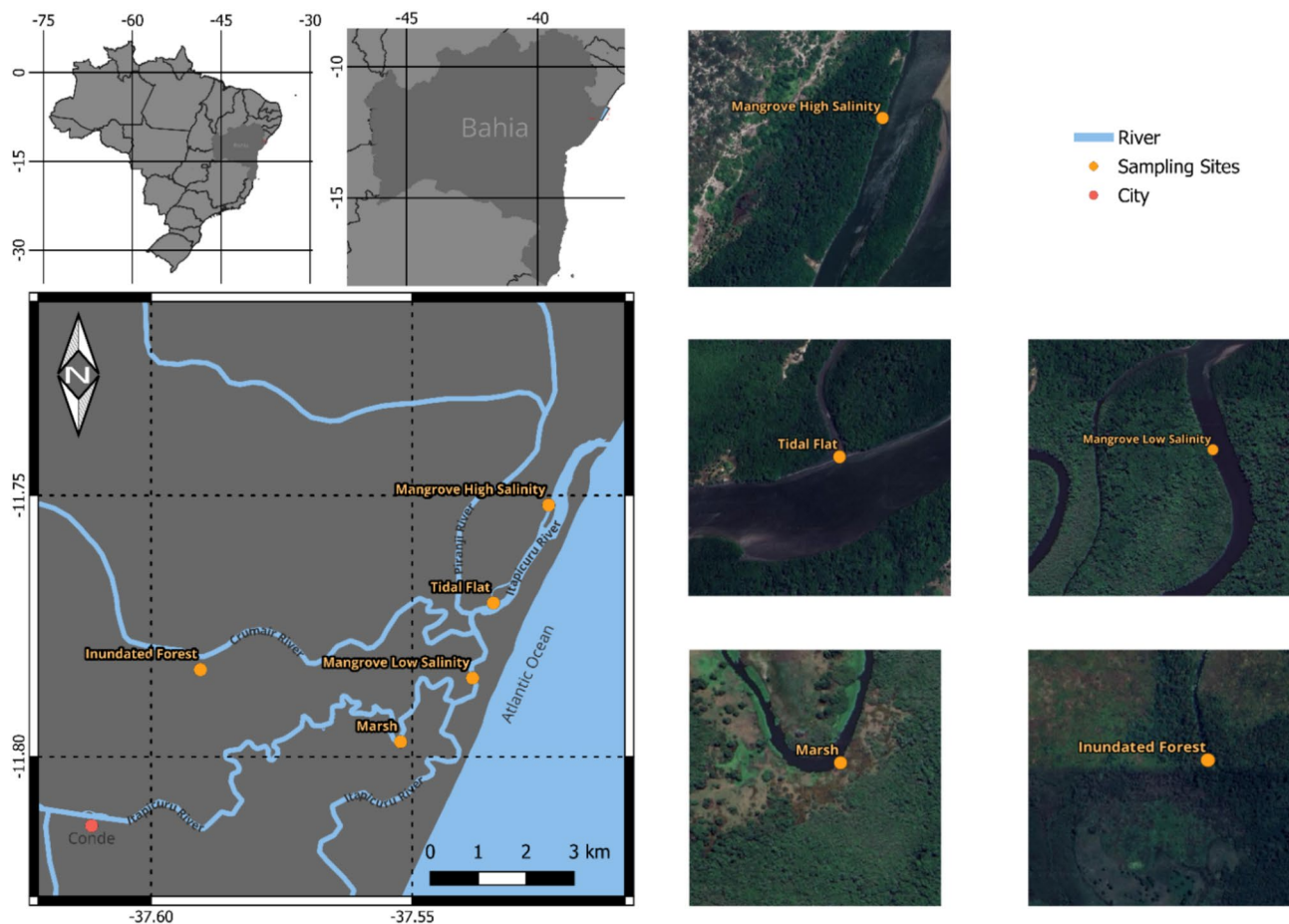


**Fig. 1.** Map showing the sampling locations of soil cores collected from various ecosystems along the Itapicuru River estuary, Northeastern Brazil. Map generated using QGIS Desktop software (Version 3.34.13, <https://qgis.org>).

The study region is part of the Atlantic Forest biome, consisting of ombrophilous forests, riparian forests, mangroves, and restinga ecosystems<sup>39</sup>. The lower estuary is dominated by mangroves, particularly *Rhizophora mangle*. In the upper estuary, the mangrove diversifies to include *Laguncularia racemosa*, *Avicennia germinans*, *A. schaueriana*, and *Conocarpus erectus*<sup>39</sup>. Marshes with *Spartina* sp., *Eleocharis* sp., and *Typha domingensis* are present upstream<sup>39</sup>. Additionally, the Conde region hosts the largest swamp forest in Bahia, which harbors more than 140 species<sup>38</sup>.

We assessed OC stocks and accumulation rates along the Itapicuru estuarine system, focusing on five distinct ecosystems (Table S1): (i) a tidal flat (TF; salinity of 15), two mangrove forests (ii) one dominated by *R. mangle* in the high salinity region of the estuary (MHS; 17 to 21), and (iii) another dominated by *R. mangle* and *L. racemosa* in the fringe forest at the lower salinity region of the estuary (MLS; 0 to 5), a (iv) freshwater marsh (MARSH; 0) dominated by *Eleocharis interstincta*, and (v) a swamp or inundated forest (INF, 0) with high terrestrial plant diversity (142 species, 67 families), dominated by Cyperaceae, followed by Polygonaceae and Myrtaceae<sup>40</sup>.

We collected 3 sediment cores using a 1 m stainless-steel open-faced auger coring device in the fringe portion of each environment (~15 m from the waterline at low tide). A transect was established parallel to the water body to avoid the potential influence of tides (intertidal position) on OC stocks and accumulation rates across ecosystems<sup>41,42</sup>. Due to operational difficulties in using the corer in poorly consolidated soils, only two soil cores were successfully recovered in the inundated forest. The lengths of the cores ranged between 70 to 100 cm, except for one corer in the inundated forest, which was only 50 cm (Table S2). All cores were sliced into 1-cm-thick layers down to a depth of 20 cm, followed by 2-cm-thick layers between depths of 20 and 50 cm, and 5-cm-thick layers beyond 50 cm to the bottom. Additionally, we collected leaves, stems and roots from the vegetation in each environment, except at INF, due to its vast diversity of terrestrial plants and at TF due to the absence of vegetation. Samples were wet weighed, frozen, freeze-dried, and reweighed to determine the dry bulk density (DBD).

### Organic carbon, total nitrogen, carbonates, and $\delta^{13}\text{C}_{\text{org}}$ and $\delta^{15}\text{N}_{\text{total}}$ analyses

Organic carbon (OC), total nitrogen (TN), and stable isotope ratios ( $\delta^{13}\text{C}_{\text{org}}$  and  $\delta^{15}\text{N}_{\text{total}}$ ) were analysed in the bulk soil fraction from all sediment slices in each core, as well as in the leaves, stems, and roots. Soil samples were

acidified with 1 M HCl to remove inorganic carbon prior to the determination of carbonate ( $C_{\text{carb}}$ ) content. OC, TN,  $\delta^{13}\text{C}_{\text{org}}$ , and  $\delta^{15}\text{N}_{\text{total}}$  were measured using a Flash 2000 elemental analyser coupled to a Delta V Advantage Isotope Ratio Mass Spectrometer (Thermo Fisher, USA). Calibration was performed using Acetanilide (OAS 1 g - Certificate 449495). Accuracy was verified using Low Organic Soil (elemental microanalysis B2153, certificate 324704) and Wheat Flour (Cat No. B2157 - Certificate No. 354738), with recovery rates exceeding 96%. The detection limits were 0.05% for OC and 0.02% for TN. Analytical precision was verified by repeated triplicate analysis, yielding a precision of  $\sim 0.1\%$  for  $\delta^{13}\text{C}_{\text{org}}$  and  $\sim 0.2\%$  for  $\delta^{15}\text{N}_{\text{total}}$ . All isotope ratio measurements are expressed relative to international reference standards, using Peedee Belemnite for  $\delta^{13}\text{C}_{\text{org}}$  and atmospheric nitrogen for  $\delta^{15}\text{N}_{\text{total}}$ .

### Grain size analysis

Grain size was measured using a laser particle diffractometer (Shimadzu model SALD-3101) following pre-treatment with HCl<sup>43,44</sup>. Samples were analysed at regular intervals: every two sediment slices in the upper 30 cm and every three slices below this depth. We classified the grain size data into two fractions sand ( $> 63 \mu\text{m}$ ) and mud, which includes both silt and clay fractions ( $< 63 \mu\text{m}$ ).

### Soil accumulation rates

The concentration profiles of  $^{210}\text{Pb}$  in each core were determined via its decay product,  $^{210}\text{Po}$ , using alpha spectrometry. This involved adding  $^{209}\text{Po}$  as an internal tracer, followed by microwave-assisted acid digestion<sup>45</sup>. Excess  $^{210}\text{Pb}$  ( $^{210}\text{Pb}_{\text{ex}}$ ) concentrations, used for age model calculations, were obtained by subtracting  $^{226}\text{Ra}$  (supported  $^{210}\text{Pb}$ ) from total  $^{210}\text{Pb}$ .  $^{226}\text{Ra}$  was measured in selected samples of each core using gamma spectrometry. As expected,  $^{226}\text{Ra}$  levels matched total  $^{210}\text{Pb}$  concentrations at depths beyond the  $^{210}\text{Pb}_{\text{ex}}$  horizons in each core. The Constant Flux:Constant Sedimentation (CF:CS) model<sup>46</sup> where applicable, was used to calculate mean mass accumulation rates (MAR, in  $\text{g cm}^{-2} \text{yr}^{-1}$ ) and sediment accumulation rates (SAR, in  $\text{mm yr}^{-1}$ ) (Table 1). Accumulation rates of OC, TN and  $C_{\text{carb}}$  were estimated by multiplying the MAR ( $\text{g cm}^{-2} \text{yr}^{-1}$ ) by the weighted average contents of the respective element in soils (% element). The accumulation period was defined based on the depth where total  $^{210}\text{Pb}$  reaches equilibrium with supported  $^{210}\text{Pb}$ .

Soil stocks (OC, TN,  $C_{\text{carb}}$ ) were calculated to a depth of 1 meter, following current literature practices<sup>47</sup>. Where data was unavailable (8 out of 14 cores), we extrapolated the stocks down to 1 meter by linearly extending the integrated values with depth. Additionally, to ensure consistency and allow for direct comparisons among all sampling sites, we also calculated soil stocks to a non-extrapolated depth of 50 cm.

### Data analysis

Because not all variables followed a normal distribution, we used the Kruskal–Wallis test followed by Dunn's test, implemented in Python with SciPy, Statsmodels, and scikit\_posthocs, to assess variability among ecosystems. To

Core ID	Length (cm)	MAR ( $\text{g cm}^{-2} \text{yr}^{-1}$ )	SAR ( $\text{mm yr}^{-1}$ )
Mangrove high salinity			
1	100	$0.43 \pm 0.03^a$	$5.24 \pm 0.42$
2	100	NA	NA
3	100	NA	NA
Mangrove low salinity			
1	100	NA	NA
2	95	$0.39 \pm 0.04^b$	$5.48 \pm 0.47$
3	95	$0.28 \pm 0.01^c$	$4.11 \pm 0.18$
Tidal flat			
1	100	$0.27 \pm 0.05^d$	$6.61 \pm 1.20$
2	92	$0.16 \pm 0.01^e$	$3.94 \pm 0.29$
3	90	$0.40 \pm 0.02^f$	$9.56 \pm 0.57$
Marsh			
1	95	$0.33^g$	4.56
2	100	$0.39 \pm 0.06^h$	$9.27 \pm 1.35$
3	70	$0.41 \pm 0.12^i$	$6.01 \pm 1.70$
Inundated forest			
1	50	$0.06^j$	4.45
2	83	$0.08^k$	8.08

**Table 1.** Mass and soil accumulation rates from each treatment soil (MAR and SAR). Although mixing along the sediment profile, excess  $^{210}\text{Pb}$  indicated relatively high accumulation of sediment. The values below should be considered as upper values estimations. Regions from which MAR and SAR were calculated using  $^{210}\text{Pb}$ : a = 20–75 cm, b = 1–40 cm, c = 7–35 cm, d = 16–26 cm, e = 26–42 cm, f = 11–34 cm, g = 40–65 cm, h = 1–70 cm, i = 4–50 cm, j = 10–30 cm, k = 40–80 cm.

explore relationships among soil properties, we performed a multivariate analysis using Principal Component Analysis (PCA). The fine fraction, carbonate content, organic carbon and nitrogen concentrations,  $\delta^{13}\text{C}$  and  $\delta^{15}\text{N}$  isotopic values, molar OC:TN ratio, dry bulk density, and OC stocks were included as quantitative variables. The five sites were treated as qualitative variables. All quantitative data were standardized to unit variance, and the PCA was carried out using the R packages FactoMineR and factoextra.

## Results

### Soil physicochemical properties

The fines content varied across ecosystems. Mangroves exhibited the lowest fines content, averaging  $21 \pm 8\%$  at low salinity and  $31 \pm 12\%$  at high salinity sites. In contrast, the marsh had an average fines content of  $44 \pm 9\%$ , the tidal flat  $59 \pm 14\%$ , and the inundated forest  $76 \pm 10\%$  (Tables S2 and S3). Along the soil profiles, fines content was relatively constant within each ecosystem (Fig. 2).

OC and TN showed significant differences across ecosystems, ranging from  $2.94 \pm 0.81\%$  to  $22.14 \pm 4.49\%$  and  $0.11 \pm 0.03\%$  to  $1.17 \pm 0.16\%$ , respectively. The Inundated Forest presented the highest OC and TN values ( $21.3 \pm 5.63\%$  and  $1.14 \pm 0.21\%$  respectively,  $p < 0.05$ ; Tables S2 and S3), followed by the Tidal Flat, which had significantly higher values than the Marsh ( $p < 0.05$ ; Tables S2 and S3). The lowest values were observed in the mangrove sites, with no significant differences in OC content between them. However, for TN, the Mangrove High Salinity showed slightly, but significantly higher values than the Mangrove Low Salinity ( $p < 0.05$ ; Table S2 and S3).

Across sediment profiles, inundated forest (INF) consistently exhibited high organic carbon (OC) and total nitrogen (TN) with no clear vertical trend, whereas Mangrove Low Salinity and Tidal Flat sites showed increasing OC and TN from the bottom to the surface. No clear trend was observed at Mangrove High Salinity and Marsh for OC values. For TN vertical profiles presented an increasing trend from the bottom towards the surface at all sites except for the mangrove High Salinity (Fig. 2). The OC:TN molar ratio differed significantly

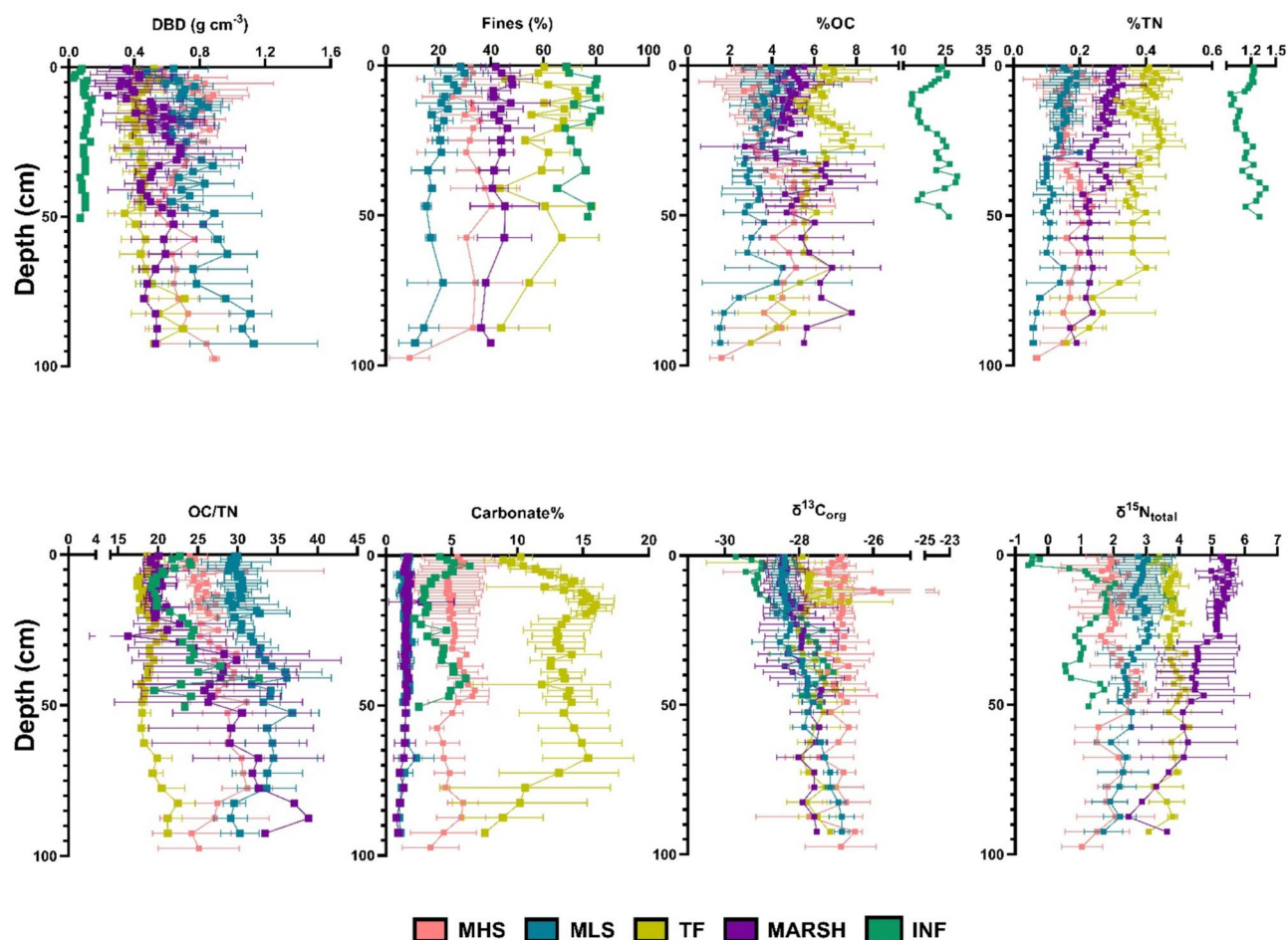


**Fig. 2.** Vertical profiles of mean ( $\pm$  standard error) OC (%), Total nitrogen (%),  $\delta^{13}\text{C}_{\text{org}}$  (‰),  $\delta^{15}\text{N}_{\text{total}}$  (‰), Fines (silt + clay;  $< 63 \mu\text{m}$ ) (%), dry bulk density, carbonate (%) and OC:TN ratio, in soils collected at Mangrove High Salinity (MHS), Mangrove Low Salinity (MLS), Tidal Flat (TF) Marsh and Inundated Forest (INF).

among ecosystems (Tidal Flat < Inundated Forest = Marsh < Mangrove High Salinity < Mangrove Low Salinity;  $p < 0.05$ ; Table S2 and S3) and ranged from  $18.6 \pm 1.4$  to  $33.3 \pm 2.9$  (Fig. 2; Table S2).

$C_{\text{carb}}$  content ranged from  $1.34 \pm 0.32\%$  to  $13.6 \pm 2.4\%$  and differed significantly among ecosystems (Mangrove Low Salinity < Marsh < Inundated Forest = Mangrove High Salinity < Tidal Flat;  $p < 0.05$ ; Table S2 and S3). Values remained low and constant in Marsh, Mangrove Low Salinity, and Mangrove High Salinity (with slight variability), while Tidal Flat and Inundated Forest showed an increase with depth, followed by stabilization and a final decrease near the surface.

$\delta^{13}\text{C}_{\text{org}}$  values ranged from  $-28.8 \pm 0.6\%$  to  $-26.6 \pm 0.9\%$ , lowest in the Inundated Forest, Marsh, and Mangrove Low Salinity and highest in Mangrove High Salinity and Tidal Flat ( $p < 0.05$ ; Tables S2 and S3). Profiles displayed decreasing  $\delta^{13}\text{C}_{\text{org}}$  toward the surface in the Mangrove Low Salinity and at the Inundated Forest. In contrast, Tidal Flat, Mangrove High Salinity, and Marsh remained relatively constant with some variability (Fig. 2).

$\delta^{15}\text{N}_{\text{total}}$  values ranged from  $0.72 \pm 0.71\%$  to  $4.68 \pm 1.00\%$ , with the lowest values at the Inundated Forest and Mangrove High Salinity sites and the highest at the Marsh, followed by the Tidal Flat and Mangrove Low Salinity ( $p < 0.05$ ; Tables S2 and S3). Vertical profiles showed slight  $\delta^{15}\text{N}_{\text{total}}$  enrichment toward the surface in Mangrove Low Salinity and Marsh soils, while Mangrove High Salinity and Tidal Flat sites displayed smaller variation. In the Inundated Forest,  $\delta^{15}\text{N}_{\text{total}}$  remained stable from the bottom to  $\sim 10$  cm depth, before declining near the surface (Fig. 2).

### Sources of stable isotopic composition

The  $\delta^{13}\text{C}_{\text{org}}$  and  $\delta^{15}\text{N}_{\text{total}}$  isotopic composition of plant tissues exhibited considerable variability, particularly for *Rhizophora mangle* at the Mangrove High Salinity site, ranging from  $-36.4$  to  $-28.3\%$  for  $\delta^{13}\text{C}_{\text{org}}$  and from  $1.7\%$  to  $3.6\%$  for  $\delta^{15}\text{N}_{\text{total}}$  (Table 4). In contrast, at the Mangrove Low Salinity site, *R. mangle* tissues varied in a narrow range from  $-31.5$  to  $-29.0\%$  for  $\delta^{13}\text{C}_{\text{org}}$  and from  $1.7$  to  $2.9\%$  for  $\delta^{15}\text{N}_{\text{total}}$ , presenting similar  $\delta^{13}\text{C}_{\text{org}}$  values to another dominant species in the same environment, *Laguncularia racemosa* ( $\delta^{13}\text{C}_{\text{org}}$ :  $-31.7$  to  $-29.0\%$ ). However, *L. racemosa* displayed greater variability in  $\delta^{15}\text{N}_{\text{total}}$  values, ranging from  $0.9$  to  $3.3\%$ . In the Marsh, *Eleocharis interstincta* tissues exhibited narrower isotopic ranges, with  $\delta^{13}\text{C}_{\text{org}}$  values between  $-29.0$  to  $-28.7\%$  and  $\delta^{15}\text{N}_{\text{total}}$  values ranging from  $4.3$  to  $4.7\%$  for (Table 4).

### Principal component analysis (PCA)

PCA (Fig. 3) revealed that the first principal component (PC1, 43% variance) was strongly associated with TN ( $r = 0.92$ ), OC ( $r = 0.85$ ), fine sediment ( $r = 0.71$ ), and negatively with DBD ( $r = -0.87$ ), while PC2 (22%) correlated with  $\delta^{15}\text{N}_{\text{total}}$  ( $r = 0.79$ ),  $C_{\text{carb}}$  ( $r = 0.58$ ) and OC:TN ( $r = -0.65$ ). PCA showed distinct clustering of soil samples by ecosystem. The Inundated Forest separated clearly from all others, driven by high OC and TN. Mangrove ecosystems overlapped substantially and were associated with DBD, OC:TN, and  $\delta^{13}\text{C}_{\text{org}}$  variability. The Marsh

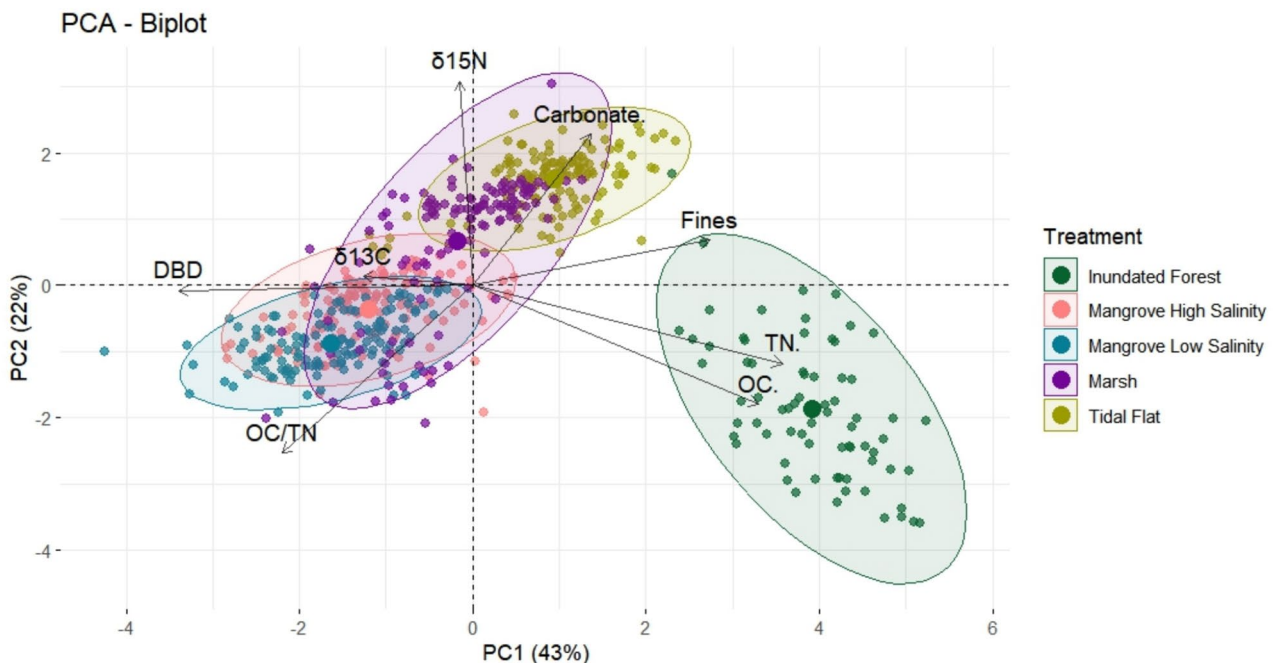


**Fig. 3.** Principal component analysis of soil properties (fine particle fraction, OC, Total N, OC:N ratio,  $\delta^{13}\text{C}_{\text{org}}$ ,  $\delta^{15}\text{N}_{\text{total}}$ , carbonate and dry bulk density) for Mangrove High Salinity, Mangrove Low Salinity, Marsh, Tidal Flat and Inundated Forest. Superimposed on the plot are the confidence ellipses for each treatment. Group mean points are represented by large circles.

overlapped with both mangroves and tidal flats and was influenced by  $C_{\text{carb}}$ ,  $\delta^{13}C_{\text{org}}$ ,  $\delta^{15}N_{\text{total}}$ , and OC:TN. Tidal flats were primarily associated with fines and  $C_{\text{carb}}$  (Fig. 3).

### $^{210}\text{Pb}$

For most sediment cores, especially Tidal Flat, excess  $^{210}\text{Pb}$  activity profiles did not show a consistent decrease with depth, indicating sediment mixing and preventing reliable age estimates for the full core length. This vertical homogenization is likely driven by sediment resuspension and bioturbation, which are common in high-energy, unvegetated environments and can obscure the expected exponential decline of  $^{210}\text{Pb}$ <sup>48</sup>. Therefore, sedimentation rate estimates (MAR and SAR) were not applied to the full core. Instead, they were calculated only for specific depth intervals where a clear decreasing trend could be identified and modelled (Table 1; Fig. 4 caption). These results should therefore be interpreted with caution and are considered as upper-limit estimates. Among the exceptions, two cores from Mangrove High Salinity and one from Mangrove Low Salinity showed intense mixing throughout the profile (Fig. 4), making rate estimates impossible. For the cores where rates could be calculated, MAR ranged from  $0.06 \text{ g cm}^{-2} \text{ yr}^{-1}$  in the Inundated Forest to  $0.43 \text{ g cm}^{-2} \text{ yr}^{-1}$  in the Mangrove High Salinity site (equivalent to  $4.45 \text{ mm yr}^{-1}$  to  $5.24 \text{ mm yr}^{-1}$ , respectively). The Marsh and Inundated Forest showed more consistent values within each ecosystem. The highest MAR was recorded in the Mangrove High Salinity site; however, this estimate was based on a single core and was similar to values from the Mangrove Low Salinity site (Table 1).

### Stocks and accumulation rates of organic carbon, nitrogen and carbonates

Stocks were calculated for the upper 50 cm (the minimum length of all cores) and also 1 m, for which some cores had to be extrapolated (see Table 1 for core lengths). The 50 cm OC stocks ranged from  $65 \text{ Mg ha}^{-1}$  at Inundated Forest to  $175 \text{ Mg ha}^{-1}$  at Marsh and did not show significant differences among ecosystems (Fig. 5; Table 2 S3), despite the large differences observed in OC content and density. For the 50 cm TN stocks, which ranged from

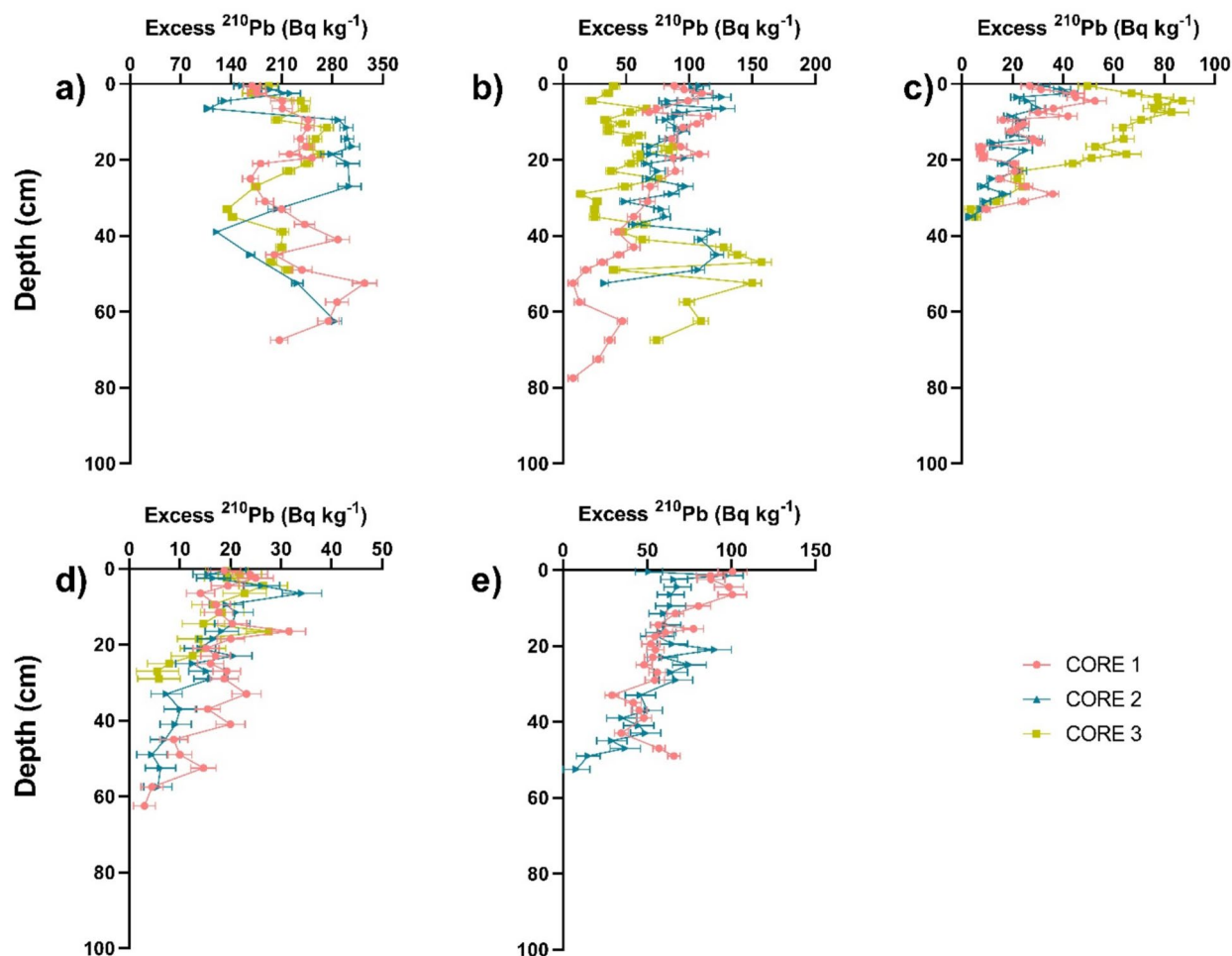


**Fig. 4.** Excess  $^{210}\text{Pb}$  specific activity profiles for soils. The depth intervals (horizons) used for MAR and SAR calculations (see Table 1) are as follows: (a) Tidal Flat: Core 1 (16–26 cm), Core 2 (26–42 cm), Core 3 (11–34 cm); (b) Mangrove High Salinity: Core 1 (20–75 cm); (c) Mangrove Low Salinity: Core 2 (1–40 cm), Core 3 (7–35 cm); (d) Marsh: Core 1 (40–65 cm), Core 2 (1–70 cm), Core 3 (4–50 cm); (e) Inundated Forest: Core 1 (10–30 cm), Core 2 (40–80 cm).

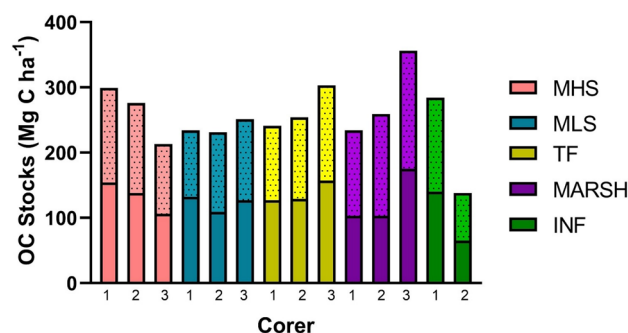


**Fig. 5.** Organic carbon stocks per replicate (1–3) core ( $\text{Mg OC ha}^{-1}$ ) across ecosystems (Mangrove High Salinity-MHS, Mangrove Low Salinity-MLS, Tidal Flat-TF, Marsh, and Inundated Forest-INF). Solid bars represent stocks up to 50 cm (measured), while dotted bars indicate stocks down to 100 cm, which for some cases had to be estimated (see Table 1 for the length of each core).

Ecosystem	Core length (cm)	Stock (50cm)			Stock (100cm)			
		OC ( $\text{Mg ha}^{-1}$ )	TN ( $\text{Mg ha}^{-1}$ )	Carbonates ( $\text{Mg ha}^{-1}$ )	OC ( $\text{Mg ha}^{-1}$ )	TN ( $\text{Mg ha}^{-1}$ )	Carbonates ( $\text{Mg ha}^{-1}$ )	
Mangrove high salinity	1	100	154	6.5	213	299	12.1	390
	2	100	138	6.3	236	276	11.9	387
	3	100	106	4.6	108	213	9.2	245
	<b>mean <math>\pm</math> sd</b>	<b>100</b>	<b>133 <math>\pm</math> 24</b>	<b>5.8 <math>\pm</math> 1.0</b>	<b>186 <math>\pm</math> 68</b>	<b>263 <math>\pm</math> 44</b>	<b>11.0 <math>\pm</math> 1.6</b>	<b>341 <math>\pm</math> 83.3</b>
Mangrove low salinity	1	100	132	4.6	51	234	8.1	104
	2	95	109	4.2	54	231*	8.8*	118*
	3	95	127	4.9	56	251*	9.2*	113*
	<b>mean <math>\pm</math> sd</b>	<b>97 <math>\pm</math> 3</b>	<b>123 <math>\pm</math> 12</b>	<b>4.6 <math>\pm</math> 0.3</b>	<b>54 <math>\pm</math> 3</b>	<b>239 <math>\pm</math> 11</b>	<b>8.7 <math>\pm</math> 0.6</b>	<b>112 <math>\pm</math> 7</b>
Tidal flat	1	100	127	7.8	271	241	14.7	520
	2	92	129	8.0	259	254*	15.8*	560*
	3	90	157	10.0	346	303*	18.9*	719*
	<b>mean <math>\pm</math> sd</b>	<b>97 <math>\pm</math> 5</b>	<b>138 <math>\pm</math> 17</b>	<b>8.6 <math>\pm</math> 1.2</b>	<b>292 <math>\pm</math> 47</b>	<b>266 <math>\pm</math> 27</b>	<b>16.4 <math>\pm</math> 2.2</b>	<b>600 <math>\pm</math> 105</b>
Marsh	1	95	103	7.1	50	234*	12.9*	102*
	2	100	103	5.1	43	259	10.3	74
	3	70	175	7.5	66	356*	15.2*	135*
	<b>mean <math>\pm</math> sd</b>	<b>88 <math>\pm</math> 16</b>	<b>127 <math>\pm</math> 42</b>	<b>6.6 <math>\pm</math> 1.3</b>	<b>53 <math>\pm</math> 12</b>	<b>283 <math>\pm</math> 64</b>	<b>11.6 <math>\pm</math> 2.6</b>	<b>106 <math>\pm</math> 30</b>
Inundated forest	1	50	140	7.5	23	284*	15.3*	44*
	2	83	65	3.5	13	138*	7.7*	27*
	<b>mean <math>\pm</math> sd</b>	<b>66</b>	<b>103</b>	<b>5.5</b>	<b>18</b>	<b>211</b>	<b>11.5</b>	<b>37</b>

**Table 2.** Organic C (OC), Total N (TN) and carbonate stocks down to 50 cm and 100 cm. Estimated values for the upper 100 cm are marked with an asterisk (\*).

3.5  $\text{Mg ha}^{-1}$  to 10  $\text{Mg ha}^{-1}$ , only the Tidal Flat had a significantly higher value compared to the Mangrove Low Salinity (Table 2, S3). In contrast, the 50 cm  $C_{\text{carb}}$  stocks exhibited high variability, ranging from 13  $\text{Mg ha}^{-1}$  to 346  $\text{Mg ha}^{-1}$  (Table 3, S3). The Tidal Flat had the highest  $C_{\text{carb}}$  stocks, followed by the Mangrove High Salinity, whereas the Mangrove Low Salinity, Marsh, and Inundated Forest had the lowest  $C_{\text{carb}}$  stocks (Table 2, S3). The 1 m OC and TN stocks followed similar patterns to those observed at 50 cm, ranging from 138  $\text{Mg ha}^{-1}$  to 356  $\text{Mg ha}^{-1}$  for OC, and from 7.7  $\text{Mg ha}^{-1}$  to 18.9  $\text{Mg ha}^{-1}$  for TN, at the Inundated Forest and the Marsh respectively (Fig 5). Likewise, the 1 m  $C_{\text{carb}}$  stocks displayed the same variability trend as those at 50 cm, ranging from 27  $\text{Mg ha}^{-1}$  at the Inundated Forest to 719  $\text{Mg ha}^{-1}$  at the Tidal Flat.

Considering that several profiles presented mixing along the cores a conservative approach was adopted to calculate the accumulation rates of OC, TN and  $C_{\text{carb}}$ . Since at least two cores were collected in each ecosystem, the lowest MAR among the cores within each ecosystem was used to estimate accumulation rates. The accumulation rates varied substantially across environments. For, OC, CAR ranged from  $94 \pm 4 \text{ g OC m}^{-2} \text{ yr}^{-1}$  at Mangrove Low Salinity to  $215 \pm 61 \text{ g OC m}^{-2} \text{ yr}^{-1}$  at Marsh. For TN, the accumulation rates ranged from  $3.6 \pm 1.4 \text{ g TN m}^{-2} \text{ yr}^{-1}$  at Mangrove Low Salinity to  $12.4 \pm 3.9 \text{ g TN m}^{-2} \text{ yr}^{-1}$  at Marsh. And the accumulation rates of  $C_{\text{carb}}$  were the lowest at Inundated Forest ( $15 \text{ g } C_{\text{carb}} \text{ m}^{-2} \text{ yr}^{-1}$ ) and the highest at Tidal Flat ( $249 \pm 18 \text{ g } C_{\text{carb}} \text{ m}^{-2} \text{ yr}^{-1}$ ) (Table 3.). The OC accumulation rates were significantly higher in the Marsh and Mangrove High Salinity, while

Core ID	Accumulation rate		
	OC (OC g m <sup>-2</sup> yr <sup>-1</sup> )	TN (TN g m <sup>-2</sup> yr <sup>-1</sup> )	Carbonate (Carbonate g m <sup>-2</sup> yr <sup>-1</sup> )
Mangrove high salinity			
1	194 ± 16	7.7 ± 2.1	238 ± 19
2	164 ± 13	7.0 ± 2.3	230 ± 19
3	202 ± 16	8.2 ± 2.4	184 ± 15
<b>mean ± sd</b>	187 ± 20	7.6 ± 0.6	217 ± 29
Mangrove low salinity			
1	105 ± 5	3.7 ± 1.4	39 ± 2
2	94 ± 4	3.6 ± 1.4	40 ± 2
3	115 ± 5	4.0 ± 1.4	42 ± 2
<b>mean ± sd</b>	105 ± 11	3.8 ± 0.2	40 ± 1.5
Tidal flat			
1	108 ± 8	6.5 ± 1.4	202 ± 15
2	105 ± 8	6.3 ± 1.2	220 ± 16
3	110 ± 8	6.9 ± 1.0	249 ± 18
<b>mean ± sd</b>	108 ± 3	6.6 ± 0.3	224 ± 24
Marsh			
1	180 ± 51	12.4 ± 3.9	87 ± 25
2	211 ± 60	10.4 ± 3.4	88 ± 25
3	215 ± 61	9.0 ± 3.0	81 ± 23
<b>mean ± sd</b>	202 ± 19	10.6 ± 1.7	85 ± 3.8
Inundated forest			
1	115	6.4	15
2	123	6.2	23
<b>mean ± sd</b>	119	6.3	19

**Table 3.** Organic carbon (OC), total N (TN) and carbonate accumulation rates for each treatment soil profiles. The accumulation rate was estimated considering the depths for which the MAR was estimated.

the Mangrove Low Salinity, Tidal Flat, and Inundated Forest exhibited lower values ( $p < 0.05$ ; Table 3. and S3). For TN accumulation, the Marsh displayed significantly higher values, followed by the Mangrove High Salinity, Tidal Flat, and Inundated Forest, which exhibited similar values, and lastly, the Mangrove Low Salinity, which showed the lowest value ( $p < 0.05$ ; Table 3. and S3). The  $C_{\text{carb}}$  accumulation rates were significantly higher in the Mangrove High Salinity and Tidal Flat, followed by the Marsh and Mangrove Low Salinity, which had similar values, while the Inundated Forest displayed the lowest  $C_{\text{carb}}$  accumulation rates ( $p < 0.05$ ; Table 3. and S3).

## Discussion

This study quantified OC stocks, accumulation rates, and stable isotope ratios across seascapes in the Itapicuru River estuary. Our results underscore the importance of a seascape-level perspective for evaluating Blue Carbon habitats, highlighting not only the distinct contribution of each ecosystem to carbon storage and long-term accumulation but also their interconnectedness in regulating organic carbon and nitrogen fluxes, including potential contributions to the ocean, which should be considered in future studies.

### OC and TN stocks across the seascape

Mangrove OC stocks reached  $263 \pm 44$  Mg OC ha<sup>-1</sup> (high salinity) and  $239 \pm 11$  Mg OC ha<sup>-1</sup> (low salinity), aligning with recent regional estimates from Brazil ( $265 \pm 149$  Mg OC ha<sup>-1</sup>)<sup>49</sup> and global averages for estuarine and marine mangroves ( $282 \pm 8.1$  and  $250 \pm 5.0$  Mg OC ha<sup>-1</sup>, respectively)<sup>27</sup>. Similarly, the marsh stored  $283 \pm 64$  Mg OC ha<sup>-1</sup>, consistent with other Brazilian marshes ( $238 \pm 213$  Mg OC ha<sup>-1</sup>)<sup>49</sup> and global estimates ( $231 \pm 38$  Mg OC ha<sup>-1</sup>)<sup>50</sup>.

The unvegetated tidal flat showed OC stocks ( $266 \pm 27$  Mg OC ha<sup>-1</sup>) comparable to those of nearby mangrove sites. Similar patterns have been reported for mudflats adjacent to fringe mangroves<sup>51</sup>, likely due to mangrove encroachment. In our case, historical satellite imagery suggests that the tidal flat was previously occupied by fringe mangroves, which retreated approximately 40 years ago. We hypothesized that OC stocks have persisted due to the high content of mud in the Tidal Flat soil which are a key factor that promotes OC trapping in this ecosystem's soils coupled with sedimentary legacy. Cross-habitat inputs and hydrodynamic transport likely also further support this persistence, highlighting the role of seascape connectivity in shaping carbon and nutrient distribution. These observations highlight that, despite the absence of vegetation, tidal flats can maintain considerable carbon stocks through physical sediment characteristics and historical ecological processes.

Tidal flats are increasingly recognized as emerging Blue Carbon ecosystems<sup>2,52,53</sup> due to their capacity for substantial carbon storage, although uncertainties regarding accumulation rates, carbon stability, and potential double counting from allochthonous inputs have limited their inclusion in formal accounting frameworks. The

tidal flat investigated here exhibited OC stocks in the upper meter exceeding the global average for similar systems (~86 Mg OC ha<sup>-1</sup>)<sup>53</sup> and similar to those reported for Pacific Coast of North America (~148 Mg OC ha<sup>-1</sup>)<sup>54</sup>. Globally, tidal flats cover an estimated 128,000 km<sup>2</sup> and store nearly 0.9 Pg C, with annual burial rates of ~130 g OC m<sup>-2</sup> yr<sup>-1</sup><sup>53</sup>, underscoring their potential relevance for coastal carbon budgets. These findings reinforce the need for further investigation of their long-term carbon stability and for their formal integration into Blue Carbon policy frameworks.

Although OC stocks estimate for the inundated forest are within the range of other ecosystems, they should be interpreted with caution due to the limited number of cores (n = 2). The soils in this ecosystem had very low dry bulk density, up to seven times lower than those in the mangroves, and exhibited high %OC, likely reflecting the presence of a thick layer of partially decomposed litter (peat). Previous studies in similar forested wetlands have reported organic layers extending from 1.5 m to as much as 4.5 m in depth<sup>55,56</sup>, suggesting that our cores were entirely contained within this organic-rich deposit.

In terms of nitrogen, TN stocks reached 11.0 ± 1.6 and 8.7 ± 0.6 Mg N ha<sup>-1</sup> in the high- and low-salinity mangroves, respectively. These values are consistent with the scarce global data available. For instance, Alongi<sup>57</sup> and Bulmer<sup>58</sup> reported up to 12.2 and 15.4 ± 1.0 Mg N ha<sup>-1</sup> in mangrove forests in Australia and New Zealand, respectively, although our values are considerably lower than the global average of ~50 Mg N ha<sup>-1</sup> reported by Alongi<sup>59</sup>. Recent studies also confirm that tropical mangroves are hotspots of nitrogen cycling, supporting intense mineralization, nitrification, and denitrification<sup>60</sup>. Similarly, the unvegetated tidal flat stored 16.4 ± 2.2 Mg N ha<sup>-1</sup> and accumulated 6.6 ± 0.3 g m<sup>-2</sup> yr<sup>-1</sup>, values comparable to vegetated Blue Carbon ecosystems, indicating their role as nutrient sinks despite lacking vegetation. This dual role in carbon and nitrogen cycling highlights their contribution to reducing nutrient export and improving coastal water quality, emphasizing the need to incorporate nitrogen alongside carbon in future Blue Carbon assessments.

These characteristics observed in the soil properties are further synthesized using a Principal Component Analysis (Fig. 3), which highlights the distinct biogeochemical clustering of the habitats. The clear separation of the Inundated Forest in PC1 likely reflects its significantly higher OC and TN contents and low DBD, emphasizing its unique soil characteristics compared to the other ecosystems. In contrast, the substantial overlap observed between the mangrove sites supports their similar soil properties and possibly common OC autochthonous sources that could not be further resolved due to the superimposed OC isotopic signature across seascapes. The intermediate position of the Tidal Flat, overlapping with both the Mangrove High Salinity and the Marsh, reflects its complex soil matrix influenced by high carbonate content and fine sediments, supporting the interpretation of mixed inputs or legacy carbon discussed previously.

### Sedimentary organic matter sources and isotopic signatures

The δ<sup>13</sup>C<sub>org</sub> and δ<sup>15</sup>N<sub>total</sub> profiles revealed differences among ecosystems, though overall, the plant tissue (i.e., leaf, branches and roots) isotopic signatures varied in a narrow range (-36.4‰ to -28.3‰ and 0.9‰ to 4.7‰, respectively). The most depleted δ<sup>13</sup>C<sub>org</sub> value (-36.4‰) was found in the root tissue of the Mangrove High Salinity site; excluding this sample, δ<sup>13</sup>C<sub>org</sub> values ranged from -32.3‰ to -28.3‰, consistent with the dominance of C<sub>3</sub> plant species across all environments. The narrow δ<sup>13</sup>C<sub>org</sub> range observed, limited the ability to clearly differentiate OM sources based on C isotopes alone (Table 4; Figure 6). This overlap aligns with previous studies in tropical coastal systems dominated by C<sub>3</sub> vegetation, where δ<sup>13</sup>C<sub>org</sub> values often fall within a restricted range and are influenced more by environmental conditions (salinity, canopy cover, and hydrology) than by vegetation type<sup>12</sup>. Moreover, a broad range of allochthonous carbon sources across seascapes is expected to contribute substantially to soil OC, often exceeding autochthonous inputs. These contributions cannot be reliably distinguished using δ<sup>13</sup>C<sub>org</sub> alone. Consequently, while our data support strong biogeochemical comparisons across the seascape, this limitation precludes a definitive evaluation of the connectivity.

In contrast, the relatively higher δ<sup>13</sup>C<sub>org</sub> values observed in the Mangrove High Salinity and Tidal Flat suggest considerable marine influence. These sites, closest to the ocean, exhibited the highest salinity levels in the study

Organic mater source	δ <sup>13</sup> C (‰)	δ <sup>15</sup> N (‰)	OC/TN
MHS leaf	-32.3	3.0	38.4
MHS branches	-28.3	1.7	142.5
MHS root	-36.4	3.6	83.7
MLS leaf/R	-31.7	2.0	30.8
MLS branches/R	-30.9	0.9	134.1
MLS root/R	-29.0	3.3	79.3
MLS leaf/L	-31.5	2.9	34.5
MLS branches/L	-29.5	1.7	135.6
MLS root/L	-28.7	2.7	97.1
MARSH leaf	-28.7	4.7	71.0
MARSH rhizome	-29.0	4.3	106.7
MARSH root	-28.7	4.4	74.7

**Table 4.** Stable isotopic composition (δ<sup>13</sup>C and δ<sup>15</sup>N) and carbon-to-nitrogen ratio (OC/TN) of tissues from Mangrove High Salinity (MHS), Mangrove Low Salinity (MLS), and MARSH ecosystems. In the low-salinity mangrove, values are shown separately for *Rhizophora mangle* (R) and *Laguncularia racemosa* (L) tissues.



## OC and TN accumulation rates

Overall, as stated above,  $^{210}\text{Pb}$ -derived MAR and SAR should be interpreted with caution, as most cores showed signs of vertical mixing that can affect the reliability of age models. Consequently, the estimated accumulation rates presented here likely represent upper-limit values, particularly in the most dynamic and unvegetated sites.

Organic carbon accumulation rates (CAR) in the mangroves presented considerable spatial variability, averaging  $105 \pm 11 \text{ g C m}^{-2} \text{ yr}^{-1}$  at Mangrove Low Salinity and  $187 \pm 20 \text{ g C m}^{-2} \text{ yr}^{-1}$  at Mangrove High Salinity (Table 3.). These rates are comparable to those previously reported for northeastern Brazil (average of  $190 \text{ g C m}^{-2} \text{ yr}^{-1}$ )<sup>49</sup> and align with global estimates ( $194 \pm 15 \text{ g C m}^{-2} \text{ yr}^{-1}$ )<sup>72</sup>. Such variability is commonly driven by both physical (e.g., tidal amplitude, salinity gradients, geomorphology and the influx of allochthonous material) and biological factors (e.g., root productivity, plant community composition, and bioturbation)<sup>1,41,73,74</sup>. Moreover, geomorphological setting plays a key role in shaping sedimentation. As shown by Adame<sup>75</sup>, riverine mangroves exhibited more uniform sediment deposition across intertidal zones, whereas tidal mangroves had greater sediment accumulation at the seaward fringe. This spatial heterogeneity in sediment accumulation rates influenced by bidirectional versus unidirectional flow regimes, affects not only the total sediment retained but also the location and extent of organic carbon transfer and sequestration across the land–seascape.

The marsh averaged  $202 \pm 19 \text{ g C m}^{-2} \text{ yr}^{-1}$ , consistent with more recent global estimates for saltmarshes of approximately  $210 \text{ g C m}^{-2} \text{ yr}^{-1}$ <sup>76</sup>. Notably, organic carbon accumulation in these ecosystems shows wide spatial variability, with reported global rates ranging from 20 to  $1700 \text{ g C m}^{-2} \text{ yr}^{-1}$ <sup>76</sup>. This variability is primarily controlled by tidal inundation regimes, especially tidal range and patterns, where higher tidal ranges often correspond to lower organic carbon contents due to enhanced soil aeration and decomposition<sup>76</sup>. In the Southwestern Atlantic, this spatial heterogeneity is also strongly influenced by local-scale drivers, including dominant plant species and biotic factors such as the presence of bioturbating organisms<sup>77</sup>. In line with Hatje<sup>49</sup>, this study contributes rare and valuable data for carbon accumulation in saltmarshes of the southwestern Atlantic, a region underrepresented in global blue carbon assessments.

Although lower, the Tidal Flat and Inundated Forest, exhibited considerable CARs ( $108 \pm 3 \text{ g C m}^{-2} \text{ yr}^{-1}$  and  $119 \text{ g C m}^{-2} \text{ yr}^{-1}$ , respectively) compared to the other blue carbon ecosystems specially the Mangrove Low Salinity site. In the Tidal Flat, accumulation is likely influenced more by sedimentary processes and legacy organic matter than by in situ primary productivity, given the absence of vegetation. Nevertheless, surrounding mangrove vegetation, hydrology, and local geomorphological conditions likely contribute to sustaining carbon burial, even in this unvegetated environment. As previously discussed, this ecosystem still shows a notable capacity to store organic carbon belowground, with OC stocks and CAR values being significant, compared to traditional blue carbon ecosystems. This highlights the need for further research on the carbon dynamics of tidal flats, which remain poorly studied. In the case of the Inundated Forest, although it supports well-developed and diverse vegetation cover, we believe that the lack of significant tidal exchange are likely key factors constraining carbon accumulation rates.

## Conclusion

This study quantified OC and TN stocks, accumulation rates, and isotopic composition across different coastal ecosystems in the Itapicuru River estuary, including both vegetated and unvegetated areas. Results show that high OC stocks are not restricted to vegetated environments. Unvegetated tidal flats also store substantial carbon, likely due to high sedimentation rates ( $108 \pm 3 \text{ g C m}^{-2} \text{ yr}^{-1}$ ), fine-grained soils, and possible legacy inputs from past mangrove coverage. Nitrogen showed similar patterns, with marshes and mangroves acting as primary sinks, while tidal flats and the inundated forest also contributed significantly to nitrogen storage, underscoring their role in nutrient retention and potential mitigation of eutrophication.

Stable isotopic data ( $\delta^{13}\text{C}_{\text{org}}$  and  $\delta^{15}\text{N}_{\text{total}}$ ) revealed the challenges of distinguishing OM sources in a predominantly C3-plant system, where isotopic ranges of potential end-members substantially overlapped. This suggests that stable isotopes alone may not provide sufficient resolution and should be complemented by additional tools such as pyrolysis analysis, fatty acids, and/or eDNA analysis.

Overall, our findings highlight the importance of including a wider range of habitats in Blue Carbon assessments. Ecosystems such as tidal flats and inland forested wetlands, as well as adjacent ocean, although often overlooked, can hold significant carbon and nitrogen stocks and contribute meaningfully to long-term carbon accumulation across seascapes. Future research should focus on the stability of these C stores, elucidating the sources and fluxes of organic carbon across habitats, and evaluating ecosystem responses to environmental change to improve carbon accounting and inform management strategies.

## Data availability

The datasets generated and/or analysed during the current study are available in the Supplementary Information files. Additional data are available from the corresponding author upon reasonable request.

Received: 27 August 2025; Accepted: 19 December 2025

Published online: 27 January 2026

## References

1. Mcleod, E. et al. A blueprint for blue carbon: Toward an improved understanding of the role of vegetated coastal habitats in sequestering CO<sub>2</sub>. *Front. Ecol. Environ.* **9**(10), 552–60 (2011).
2. Lovelock, C. E. & Duarte, C. M. Dimensions of blue carbon and emerging perspectives. *Biol. Lett.* **15**(3), 20180781 (2019).
3. Macreadie, P. I. et al. The future of blue carbon science. *Nat. Commun.* **10**(1), 3998 (2019).
4. Alongi, D. M. Carbon cycling and storage in mangrove forests. *Annu. Rev. Mar. Sci.* **6**, 195–219 (2014).

5. Duarte, C. M., Middelburg, J. J. & Caraco, N. Major role of marine vegetation on the oceanic carbon cycle. *Biogeosciences*. **2**(1), 1–8 (2005).
6. Duarte, C. M., Losada, I. J., Hendriks, I. E., Mazarrasa, I. & Marbà, N. The role of coastal plant communities for climate change mitigation and adaptation. *Nat. Clim. Chang.* **3**(11), 961–8 (2013).
7. Chen, G. C., Tam, N. F. Y. & Ye, Y. Summer fluxes of atmospheric greenhouse gases N<sub>2</sub>O, CH<sub>4</sub> and CO<sub>2</sub> from mangrove soil in South China. *Sci. Total Environ.* **408**(13), 2761–7 (2010).
8. Chen, G. et al. Soil greenhouse gas emissions reduce the contribution of mangrove plants to the atmospheric cooling effect. *Environ. Res. Lett.* **11**(12), 124019 (2016).
9. Pendleton, L. et al. Estimating global “Blue carbon” emissions from conversion and degradation of vegetated coastal ecosystems. *PLOS One* **7**(9), e43542 (2012).
10. Fu, C. et al. Stocks and losses of soil organic carbon from Chinese vegetated coastal habitats. *Glob. Chang. Biol.* **27**(1), 202–14 (2021).
11. Santos-Andrade, M., Hatje, V., Arias-Ortiz, A., Patire, V. F. & da Silva, L. A. Human disturbance drives loss of soil organic matter and changes its stability and sources in mangroves. *Environ. Res.* **202**, 111663 (2021).
12. Bouillon, S., Connolly, R. M. & Lee, S. Y. Organic matter exchange and cycling in mangrove ecosystems: Recent insights from stable isotope studies. *J. Sea. Res.* **59**(1), 44–58 (2008).
13. Cabral, A. et al. Large porewater-derived carbon outwelling across mangrove seascapes revealed by radium isotopes. *J. Geophys. Res. Ocean.* **129**(9), e2024JC021319 (2024).
14. Adame, M. F. & Lovelock, C. E. Carbon and nutrient exchange of mangrove forests with the coastal ocean. *Hydrobiologia.* **663**(1), 23–50 (2011).
15. Maher, D. T., Santos, I. R., Golsby-Smith, L., Gleeson, J. & Eyre, B. D. Groundwater-derived dissolved inorganic and organic carbon exports from a mangrove tidal creek: The missing mangrove carbon sink? *Limnol. Oceanogr.* **58**(2), 475–88 (2013).
16. Santos, I. R. et al. The renaissance of Odum’s outwelling hypothesis in “Blue Carbon” science. *Estuar. Coast. Shelf. Sci.* **5**(255), 107361 (2021).
17. Cabral, A. et al. Tidally driven porewater exchange and diel cycles control CO<sub>2</sub> fluxes in mangroves on local and global scales. *Geochim. Cosmochim. Acta.* **1**(374), 121–35 (2024).
18. Reithmaier, G. M. S. et al. Carbonate chemistry and carbon sequestration driven by inorganic carbon outwelling from mangroves and saltmarshes. *Nat. Commun.* **14**(1), 8196 (2023).
19. Robertson, A. I. Leaf-burying crabs: Their influence on energy flow and export from mixed mangrove forests (*Rhizophora* spp.) in northeastern Australia. *J Exp Mar Biol Ecol.* **102**(2), 237–48 (1986).
20. Robertson, A. I. & Daniel, P. A. The influence of crabs on litter processing in high intertidal mangrove forests in tropical Australia. *Oecologia.* **78**(2), 191–8 (1989).
21. Saavedra-Hortua, D., Nagelkerken, I., Estupinan-Suarez, L. M. & Gillis, L. G. Effects of connectivity on carbon and nitrogen stocks in mangrove and seagrass ecosystems. *Sci. Total Environ.* **20**(896), 164829 (2023).
22. Asplund, M. E. et al. Dynamics and fate of blue carbon in a mangrove–seagrass seascape: Influence of landscape configuration and land-use change. *Landscape Ecol.* **36**(5), 1489–509 (2021).
23. Chen, G. et al. Mangroves as a major source of soil carbon storage in adjacent seagrass meadows. *Sci. Rep.* **7**(1), 42406 (2017).
24. Saavedra-Hortua, D. A., Friess, D. A., Zimmer, M. & Gillis, L. G. Sources of particulate organic matter across mangrove forests and adjacent ecosystems in different geomorphic settings. *Wetlands.* **40**(5), 1047–59 (2020).
25. Cahoon, D. R., McKee, K. L. & Morris, J. T. How plants influence resilience of salt marsh and mangrove Wetlands to sea-level rise. *Est. Coast.* **44**(4), 883–98 (2021).
26. Prasad, M. B. K., Kumar, A., Ramanathan, A. L. & Datta, D. K. Sources and dynamics of sedimentary organic matter in Sundarban mangrove estuary from Indo-Gangetic delta. *Ecol. Process.* **6**(1), 8 (2017).
27. Zhang, J. et al. A global assessment of mangrove soil organic carbon sources and implications for blue carbon credit. *Nat. Commun.* **15**(1), 8994 (2024).
28. Rovai, A. S. et al. Global controls on carbon storage in mangrove soils. *Nat. Clim. Chang.* **8**(6), 534–8 (2018).
29. Twilley, R. R., Rovai, A. S. & Riul, P. Coastal morphology explains global blue carbon distributions. *Front. Ecol. Environ.* **16**(9), 503–8 (2018).
30. Yousaf, A. et al. Nitrogen dynamics in Wetland systems and its impact on biodiversity. *Nitrogen.* **2**(2), 196–217 (2021).
31. Reddy, K.R. & Graetz, D.A. Carbon and nitrogen dynamics in wetland soils. In *The Ecology and Management of Wetlands Ecology of Wetlands* (Eds Hook, D.D., McKee, W.H., Smith, H.K., Gregory, J., Burrell, V.G., DeVoe, M.R. et al.) Volume 1 307–18 [Internet], [cited 2025 Aug 26], Available from: [https://doi.org/10.1007/978-1-4684-8378-9\\_26](https://doi.org/10.1007/978-1-4684-8378-9_26) (New York, NY: Springer US, 1988).
32. Herbert, R. A. Nitrogen cycling in coastal marine ecosystems. *FEMS Microbiol. Rev.* **23**(5), 563–90 (1999).
33. Qin, L. & Liu, Y. Aerobic granulation for organic carbon and nitrogen removal in alternating aerobic–anaerobic sequencing batch reactor. *Chemosphere.* **63**(6), 926–33 (2006).
34. Fulton, C. J. et al. Tracing blue carbon flows across diverse seascapes. *Glob. Chang. Biol.* **31**(8), e70420 (2025).
35. Companhia de Desenvolvimento dos Vales do São Francisco e do Parnaíba Codevasf RLXN, Modificação 24/06/2021 10h21 Ú. Itapicuru [Internet]. Companhia de Desenvolvimento dos Vales do São Francisco e do Parnaíba Codevasf. Available from: <https://www.codevasf.gov.br/ acesso-a-informacao/institucional/area-de-atuacao/bacia-hidrografica/itapicuru> [cited 2025 Aug 26] (2025).
36. Guimarães, L.M., Lima de T. A.C., França, E.J.D., Arruda de, G.N., Souza de, J.R.B., Albergaria-Barbosa de, A.C.R., Impacts of local vegetation changes in the organic matters input for a preserved tropical estuary (Itapicuru - BA River Estuary). *Quím Nova.* **42** 611–8 (2019).
37. Barbosa Júnior, E.C., Silva, F.L.G.D., Meira, V.H., Morato, K., Gottschalk, E., Rosa, G.D.L. et al The influence of small human settlements on marine litter in the northeast coast of Brazil. *Rev. Gest. Costeira Integrada.* 181 93 (2019).
38. Nunes de, J.M.C., Matos de, M.R.B., Litoral norte da Bahia: Caracterização ambiental, biodiversidade e conservação (2017).
39. de Santana, J. S. et al. Fontes de matéria orgânica para os sedimentos superficiais do estuário do rio itapicuru (bahia - brasil). *Quím. Nova.* **46**(608), 15 (2023).
40. Menezes, C.M., Aguiar de, L.G.P.A., Espinheira, M.J.C.L., Silva VÍs da. Florística e Fitossociologia do componente arbóreo do município de Conde, Bahia, Brasil. *Rev. Biociências*, **15**(1) Available from: <https://periodicos.unitau.br/biociencias/article/view/816> [cited 2025 Nov 3] (2009).
41. Hatje, V., Masqué, P., Patire, V. F., Dórea, A. & Barros, F. Blue carbon stocks, accumulation rates, and associated spatial variability in Brazilian mangroves. *Limnol. Oceanogr.* **66**(2), 321–34 (2021).
42. Jatobá-Junior, A. A. et al. Carbon and mercury burial in mangrove soils across an anthropogenic gradient. *Estuar. Coast. Shelf. Sci.* **15**(318), 109226 (2025).
43. Blott, S. J., Croft, D. J., Pye, K., Saye, S. E. & Wilson, H. E. Particle size analysis by laser diffraction. *Geol Soc Lond Spec Publ.* **232**(1), 63–73 (2004).
44. McCave, I.N., Bryant, R.J., Cook, H.F., Coughanowr, C.A. Evaluation of a laser-diffraction-size analyzer for use with natural sediments. *Res. Method. Paper. J. Sedim. Res.* **56**(4). Available from: <https://archives.datapages.com/data/sepm/journals/v55-58/dat/056/056004/0561.htm> [cited 2025 Aug 26] (1986).
45. Sanchez-Cabeza, J., Masqué, P., Ani-Ragolta, I. 210Pb and 210Po analysis in sediments and soils by microwave acid digestion. 2006 Apr 12 Available from: <https://akjournals.com/view/journals/10967/227/1-2/article-p19.xml> [cited 2025 Aug 26] (2006).

46. Krishnaswamy, S., Lal, D., Martin, J. M. & Meybeck, M. Geochronology of lake sediments. *Earth Planet Sci. Lett.* **11**(1), 407–14 (1971).
47. Howard, J., Hoyt, S., Isensee, K., Telszewski, M., Pidgeon, E. Coastal blue carbon: Methods for assessing carbon stocks and emissions factors in mangroves, tidal salt marshes, and seagrasses Available from: <https://hdl.handle.net/10568/95127> (2014).
48. Arias-Ortiz, A. et al. Reviews and syntheses: <sup>210</sup>Pb-derived sediment and carbon accumulation rates in vegetated coastal ecosystems – setting the record straight. *Biogeosciences*. **15**(22), 6791–818 (2018).
49. Hatje, V. et al. Vegetated coastal ecosystems in the Southwestern Atlantic ocean are an unexploited opportunity for climate change mitigation. *Commun. Earth Environ.* **4**(1), 160 (2023).
50. Maxwell, T. L. et al. Global dataset of soil organic carbon in tidal marshes. *Sci. Data*. **10**(1), 797 (2023).
51. Sasmito, S. D. et al. Organic carbon burial and sources in soils of coastal mudflat and mangrove ecosystems. *Catena*. **1**(187), 104414 (2020).
52. Howard, J. et al. Blue carbon pathways for climate mitigation: Known, emerging and unlikely. *Mar. Polic.* **1**(156), 105788 (2023).
53. Chen, Z.L., Lee, S.Y. Tidal flats as a significant carbon reservoir in global coastal ecosystems. *Front. Mar. Sci.* **9** Available from: <https://www.frontiersin.org/journals/marine-science/articles/https://doi.org/10.3389/fmars.2022.900896/full> [cited 2025 Aug 26] (2022).
54. Janousek, C. N. et al. Blue carbon stocks along the pacific coast of North America are mainly driven by local rather than regional factors. *Glob. Biogeochem. Cycle*. **39**(3), 8239 (2025).
55. Novita, N., Kauffman, J.B., Hergoualc'h, K., Murdiyarto, D., Tryanto, D.H., Jupesta, J. Carbon stocks from peat swamp forest and oil palm plantation in central Kalimantan, Indonesia. In *Climate Change Research, Policy and Actions in Indonesia: Science, Adaptation and Mitigation* (eds Djalante, R., Jupesta, J., Aldrian, E.) 203–27, Available from: [https://doi.org/10.1007/978-3-030-55336-8\\_10](https://doi.org/10.1007/978-3-030-55336-8_10) [cited 2025 Aug 26] (Cham, Springer International Publishing, 2021).
56. Jaenicke, J., Rieley, J. O., Mott, C., Kimman, P. & Siebert, F. Determination of the amount of carbon stored in Indonesian peatlands. *Geoderma*. **147**(3), 151–8 (2008).
57. Alongi, D. M., Clough, B. F., Dixon, P. & Tirendi, F. Nutrient partitioning and storage in arid-zone forests of the mangroves *Rhizophora stylosa* and *Avicennia marina*. *Trees*. **17**(1), 51–60 (2003).
58. Bulmer, R.H., Schwendenmann, L., Lundquist, C.J. Carbon and nitrogen stocks and below-ground allometry in temperate mangroves. *Front. Mar. Sci.* **3** Available from: <https://www.frontiersin.org/journals/marine-science/articles/https://doi.org/10.3389/fmars.2016.00150/full> [cited 2025 Aug 26] (2016).
59. Alongi, D. M. Nitrogen cycling and mass balance in the world's mangrove forests. *Nitrogen*. **1**(2), 167–89 (2020).
60. Adame, M. F., Iram, N., Gamboa-Cutz, J. N. & Masque, P. Nitrogen processes within tropical mangroves in Australia. *J. Geophys. Res.* **130**(4), e2024JG008335 (2025).
61. Lamb, A. L., Wilson, G. P. & Leng, M. J. A review of coastal palaeoclimate and relative sea-level reconstructions using  $\delta^{13}\text{C}$  and C/N ratios in organic material. *Earth-Sci. Rev.* **75**(1), 29–57 (2006).
62. Kennedy, H., Beggins, J., Duarte, C.M., Fourqurean, J.W., Holmer, M., Marbà, N. et al. Seagrass sediments as a global carbon sink: Isotopic constraints. *Glob. Biogeochem. Cycle*. **24**(4) Available from: <https://onlinelibrary.wiley.com/doi/abs/https://doi.org/10.1029/2010GB003848> [cited 2025 Nov 4] (2010).
63. Saintilan, N., Rogers, K., Mazumder, D. & Woodroffe, C. Allochthonous and autochthonous contributions to carbon accumulation and carbon store in southeastern Australian coastal wetlands. *Estuar. Coast. Shelf. Sci.* **10**(128), 84–92 (2013).
64. Kristensen, E., Bouillon, S., Dittmar, T. & Marchand, C. Organic carbon dynamics in mangrove ecosystems: A review. *Aquat. Bot.* **89**(2), 201–19 (2008).
65. Heaton, T. H. E. Isotopic studies of nitrogen pollution in the hydrosphere and atmosphere: A review. *Chem. Geol. Isot. Geosci. Sect.* **1**(59), 87–102 (1986).
66. Koba, K. et al.  $\delta^{15}\text{N}$  of soil N and plants in a N-saturated, subtropical forest of southern China. *Rapid. Commun. Mass Spectrom.* **24**(17), 2499–506 (2010).
67. Craine, J. M. et al. Ecological interpretations of nitrogen isotope ratios of terrestrial plants and soils. *Plant Soil*. **396**(1), 1–26 (2015).
68. Chapin FS, Matson PA, Mooney HA, editors. Terrestrial production processes. In. *Principles of Terrestrial Ecosystem Ecology* 123–50 Available from: [https://doi.org/10.1007/0-387-21663-4\\_6](https://doi.org/10.1007/0-387-21663-4_6) [cited 2025 Aug 26] (New York, NY, Springer, 2002).
69. Cornelissen, J. H. C. et al. Leaf structure and defence control litter decomposition rate across species and life forms in regional floras on two continents. *New. Phytol.* **143**(1), 191–200 (1999).
70. Silver, W. L. & Miya, R. K. Global patterns in root decomposition: Comparisons of climate and litter quality effects. *Oecologia*. **129**(3), 407–19 (2001).
71. Capel, E. L., de la Rosa Arranz, J. M., González-Vila, F. J., González-Perez, J. A. & Manning, D. A. C. Elucidation of different forms of organic carbon in marine sediments from the Atlantic coast of Spain using thermal analysis coupled to isotope ratio and quadrupole mass spectrometry. *Org. Geochem.* **37**(12), 1983–94 (2006).
72. Wang, F. et al. Global blue carbon accumulation in tidal wetlands increases with climate change. *Natl. Sci. Rev.* **8**(9), nwa0296 (2021).
73. Amundson, R. The carbon budget in soils. *Annu. Rev. Earth Planet Sci.* **29**(29), 535–62 (2001).
74. Kauffman, J. B. et al. Carbon stocks of mangroves and salt marshes of the Amazon region. *Brazil. Biol. Lett.* **14**(9), 20180208 (2018).
75. Adame, M. F., Neil, D., Wright, S. F. & Lovelock, C. E. Sedimentation within and among mangrove forests along a gradient of geomorphological settings. *Estuar. Coast. Shelf. Sci.* **86**(1), 21–30 (2010).
76. Huyzentruyt, M., Belliard, J. P., Saintilan, N. & Temmerman, S. Identifying drivers of global spatial variability in organic carbon sequestration in tidal marsh sediments. *Sci. Total Environ.* **20**(957), 177746 (2024).
77. Martinetto, P. et al. The blue carbon of southern southwest Atlantic salt marshes and their biotic and abiotic drivers. *Nat. Commun.* **14**(1), 8500 (2023).

## Acknowledgements

This work was supported by CNPq (407297/2018-9) and FAPESB (APP0012/2023). The authors were sponsored by FAPESB (A.A.J.J.) and CNPq (V.H., 302477/2022-5). The IAEA is grateful for the support provided to its Marine Environment Laboratories by the Government of the Principality of Monaco. We also thank André Rovai and Alex Cabral for their valuable feedback on an earlier draft of this manuscript; Yuri Hoya, Karol Ferreira, and Eduardo Mendes for field assistance; and Prof. Lenise Guedes for identifying the plant species. We also thank Inés Sanz-Álvarez and Beat Gasser for their assistance with the analyses.

## Author contributions

V.H. and A.A.J.J. conceived the study. V.H. acquired funding, performed data analysis, and drafted the original manuscript. A.A.J.J. contributed to data analysis, drafting, and manuscript revision. P.M. and C.E.R. contributed to data production, data interpretation, and manuscript revision. All authors revised and approved the final version of the manuscript.

## Funding

This work was supported by CNPq (407297/2018-9) and FAPESB (APP0012/2023). The authors were sponsored by FAPESB (A.A.J.J.) and CNPq (V.H., 302477/2022-5).

## Declarations

## Competing interests

The authors declare no competing interests.

## Additional information

**Supplementary Information** The online version contains supplementary material available at <https://doi.org/10.1038/s41598-025-33546-x>.

**Correspondence** and requests for materials should be addressed to A.A.J.-J.

**Reprints and permissions information** is available at [www.nature.com/reprints](http://www.nature.com/reprints).

**Publisher's note** Springer Nature remains neutral with regard to jurisdictional claims in published maps and institutional affiliations.

**Open Access** This article is licensed under a Creative Commons Attribution-NonCommercial-NoDerivatives 4.0 International License, which permits any non-commercial use, sharing, distribution and reproduction in any medium or format, as long as you give appropriate credit to the original author(s) and the source, provide a link to the Creative Commons licence, and indicate if you modified the licensed material. You do not have permission under this licence to share adapted material derived from this article or parts of it. The images or other third party material in this article are included in the article's Creative Commons licence, unless indicated otherwise in a credit line to the material. If material is not included in the article's Creative Commons licence and your intended use is not permitted by statutory regulation or exceeds the permitted use, you will need to obtain permission directly from the copyright holder. To view a copy of this licence, visit <http://creativecommons.org/licenses/by-nc-nd/4.0/>.

© The Author(s) 2026